Journal of GeoEngineering, Vol. 18, No. 3, pp. 103-116, September 2023
http://dx.doi.org/10.6310/jog.202309_18(3).2

NUMERICAL EVALUATION ON THE APPLICATION OF SMALL STRAIN STIFFNESS MODEL FOR DEEP EXCAVATIONS IN SOFT CLAYS

Yu-Xuan Li [1], Ari Surya Abdi [2*], Fuchen Teng [3], and Chang-Yu Ou [4]

ABSTRACT

The finite element method is commonly used to conduct the excavation project and to ensure the safety of the adjacent building. Hence, the analysis method should be rigorous, and the soil parameters used in the analysis should be carefully determined. In this paper, a small strain stiffness model was performed to assess the influence of small-strain soil behavior on ground movement induced by deep excavation in soft clays. The results revealed that when the stiff soil is far away from the excavation base, the hardening small strain model should be used to obtain a better prediction. On the other hand, the ground movement is restrained by the stiff soil when the location of stiff soil is near the excavation base. Under such conditions, the results from hardening soil and hardening small strain models are similar. In addition, this paper also provides a method to determine the small strain parameters (shear modulus and shear strain). Furthermore, the analysis method was verified through several case histories in Taipei and San Francisco. The results from case studies concluded that the small strain parameter should be determined by considering soil conditions and construction methods.

Key words: deep excavation, finite element method, hardening soil model, small strain stiffness, soft clay, ground movement.

1. INTRODUCTION

The estimation of wall displacement and ground settlement induced by deep excavation is crucial in an urban area. Accordingly, the analysis method and design concept for the deep excavation problem should be rigorous and carefully conducted. In practice, the total stress soil model is generally used to simulate undrained soil because its parameters can be simply obtained by the conventional soil test. However, it is important to note that the determination of the stiffness parameter in this soil model is highly empirical and unable to predict the actual soil behavior well (Lim *et al.* 2010; Ou 2015). Thus, the effective stress soil model is preferred because this model has a more solid theoretical formulation, while the soil behavior is governed by the effective stress rather than total stress (Lim *et al.* 2010). In such conditions, a more advanced soil constitutive model, such as Hardening soil (HS) and Hardening with small-strain (HSS) soil model, could be considered in analyses, which could simulate a more realistic soil behavior.

In recent years, the HS soil model (Schanz *et al.* 1999; Khoiri and Ou 2013; Hsieh and Ou 2018; Yeh *et al.* 2022) is often used to analyze deep excavation problems because it can provide a more reasonable unloading-reloading stiffness behavior, hardening effect, and stress-dependent on soil stiffness. Although the HS model is well adopted in the geotechnical analysis, it does not consider the characteristics of soil stiffness under small strains condition. In fact, the soil stiffness would be higher as the shear strain becomes smaller. Benz (2007) developed a soil model that can simulate the non-linear of small strain soil behavior based on the HS model, so-called the hardening small-strain soil model (HSS model). This problem becomes important because the analysis performed by the HS model could overestimate the ground movement at small strain conditions (Ou *et al.* 2013; Lim and Ou 2017).

In this study, the characteristic of wall displacement and ground settlement induced by deep excavation was evaluated by using the two and three-dimensional finite element method with considering the small strain soil behavior. The parametric case was initially performed to evaluate the characteristics of small strain behavior in deep excavations. Furthermore, several excavation cases were analyzed to verify the analysis method, including the Taipei National Enterprise Center (TNEC), Taipei Gas Company, San Francisco, Uni-President International Building (UPIB), and Wenlinyuan cases.

2. CHARACTERISTICS AND PARAMETERS OF SMALL STRAIN BEHAVIOR

In deep excavation analysis, the prediction of ground settlement in the secondary impact zone (SIZ) without considering the small strain behavior usually overestimates the field monitoring (Lim *et al.* 2010; Lim and Ou 2017). This is because the soil located far behind the wall (*e.g.,* three to five times of excavation depth, 3-5H_e) has very small ground movement in actual condition (*i.e.,* small-strain condition). Besides, the actual soil stiffness will decrease non-linearly with the increase of the shear strain. Under such conditions, the HSS soil model is rather than the HS model

Manuscript received April 4, 2023; revised May 18, 2023; accepted May 21, 2023.
[1] Former Master student, Department of Civil and Construction Engineering, National Taiwan University of Science and Technology, Taiwan.
[2*] Ph.D. Candidate (corresponding author), Department of Civil and Construction Engineering, National Taiwan University of Science and Technology, Taiwan. (e-mail: arisuryaabdi.asa@gmail.com).
[3] Associate Professor, Department of Civil and Construction Engineering, National Taiwan University of Science and Technology, Taiwan.
[4] Professor, Department of Civil and Construction Engineering, National Taiwan University of Science and Technology, Taiwan.

in simulating the real soil behavior at a small strain level, which could accurately predict the wall displacement and ground settlement induced by deep excavations.

According to the soil test data from the previous studies (Hardin and Drnevich 1972; Santos and Correia 2001), the shear modulus tends to decrease non-linearly at a certain range of strain levels. In such a case, the formulation of small strain stiffness can be defined based on the modulus reduction curves, where the shear modulus (G) is plotted as a logarithmic function of the shear strain (γ) (Brinkgreve *et al.* 2007). The shear strain herein ranges from very small strain levels (*e.g.,* vibrations or dynamic methods) up to large strain levels (*e.g.,* conventional soil testing). The modulus reduction curve is characterized by the shear modulus at a small strain level (G_0) and the shear strain level ($\gamma_{0.7}$) at which the shear modulus (G) is reduced to 70% of G_0 value, which can be expressed as:

$$G = \frac{G_0}{1 + a\left(\frac{\gamma}{\gamma_{0.7}}\right)} \tag{1}$$

where a can be given as 0.385 to give the best fit of the test data conducted by the previous studies (Santos and Correia 2001). The application of Eq. (1) is illustrated in Fig. 1.

Many researchers have studied the small-strain behavior of soil through the finite element and experimental studies (Shibuya and Tanaka 1999; Benz 2007; Lim and Ou 2017). For example, Teng (2010) conducted a series of K_0-consolidated undrained triaxial compression (CK_0UC) tests with multi-orientation bender element tests to evaluate the stiffness anisotropy of Taipei silty clay. The anisotropy ratio of the shear modulus thus obtained, which was varied from a very small strain to failure. The results showed that the normalized small strain shear modulus (G_0/P_a) was enhanced as the normalized mean effective stress increased (p'/P_a), as plotted in Fig. 2. The regression line was adopted to determine the shear modulus at small strain for analysis, which can be expressed as:

$$G_0 / P_a = 415.85\,(p'/P_a)^{0.7057} \tag{2}$$

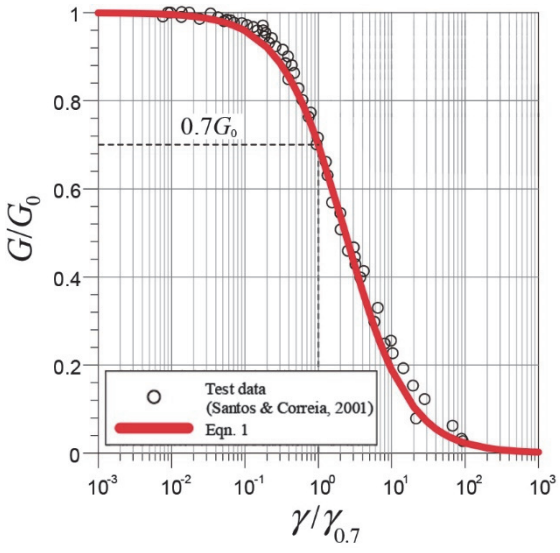

Fig. 1 Reduction of shear modulus with shear strain

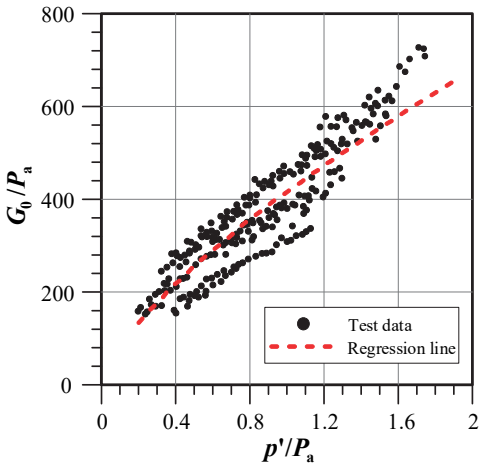

Fig. 2 Relationship between the small strain shear modulus and mean effective stress of Taipei silty clay (Teng 2010)

where p' is the mean effective stress; and P_a is the atmospheric pressure (P_a = 100 kPa).

In addition, Hardin and Black (1969) conducted the resonant column test to measure the shear modulus for various soils, taking into account both isotropic and anisotropic conditions. An empirical formula was then proposed based on the collected test data, which can be defined by the correlation of the initial void ratio (e) and the reference small-strain shear modulus (G_0^{ref}). Therefore, this relation can be expressed by the following formula:

$$G_0^{ref} = (15.75\sim33)\frac{(2.973-e)^2}{(1+e)}\ \text{[MPa]} \quad \text{for } p^{ref} = 100\ \text{kPa} \tag{3}$$

where e is void ratio; p^{ref} = 100 kPa is the reference pressure equal to the atmospheric pressure; 15.7 and 33 are the limits of the empirical soil parameter, the upper limit (33) is used in the analysis because the soil is disturbed during excavation, so the void ratio will be greater than that of soil drilling sampling.

3. PARAMETRIC STUDY ON THE APPLICATION OF SMALL STRAIN PARAMETERS

In this section, a parametric study was conducted to evaluate the influence of small strain parameters on the wall displacement, ground settlement, and soil heave induced by deep excavations. A series of two-dimensional (2D) finite element analyses were conducted by using the commercial geotechnical software PLAXIS (Brinkgreve *et al.* 2013). The typical TNEC excavation case (Ou *et al.* 2000; Lim *et al.* 2010) was adopted as the parametric case to represent the general behavior of Taipei silty clay by considering the small strain behavior. Different types of soil models (*i.e.,* HS and HSS soil models) were adopted in the analyses. In addition, the distribution of shear modulus around the excavation zone was also introduced, which ranged by strain levels.

3.1 Determination of Soil Parameters

This study modeled the clay layer as undrained material, while the sand layer was assumed to be drained. In general, there

are three different types of stiffness parameters in the HS and HSS model, such as the reference secant stiffness (E_{50}^{ref}), the reference for primary oedometer loading (E_{oed}^{ref}), and the reference unloading-reloading stiffness (E_{ur}^{ref}). The terms "reference" herein refer to the reference stress (p^{ref} = 100 kPa).

For the sand layer, the modulus soil parameters were initially estimated by using Eq. (4), which is based on the correlation of N-SPT value (Khoiri and Ou 2013). Furthermore, the E_s value was converted to E_{ur}^{ref} in order to be used as an input parameter for the HS model, as shown in Eq. (5). The other reference stiffness parameters were assumed to be $E_{50}^{ref} = E_{ur}^{ref}/3$ and $E_{oed}^{ref} = E_{50}^{ref}$ (Schanz and Vermeer 1998; Calvello and Finno 2004).

$$E_s = (2000 \sim 4000) N_{SPT} \quad [\text{kPa}] \tag{4}$$

$$E_{ur}^{ref} = \frac{E_s}{(\sigma'_3 / p^{ref})^m} \tag{5}$$

where E_s is Young's modulus of coarse-grained soils (E_s = 3000 N_{SPT} was used for analysis); σ'_3 is the minor principal stress; the power m represents the amount of stress dependency, and for clay and sand soils, it can be taken as 1.0 and 0.5, respectively (Schanz *et al.* 1999; Lim *et al.* 2016).

For the clay layer, the reference unloading-reloading stiffness (E_{ur}^{ref}) was obtained by using Eq. (6), which is based on the swelling index (C_s) obtained by the oedometer test (Lim *et al.* 2010; Hsieh and Ou 2018). The other reference stiffness parameters were assumed to be $E_{50}^{ref} = E_{ur}^{ref}/3$ and $E_{oed}^{ref} = 0.7\ E_{50}^{ref}$, as suggested by Calvello and Finno (2004).

$$E_{ur}^{ref} = \frac{3(1+e_0) p^{ref} (1-2\nu_{ur})}{\kappa} \tag{6}$$

where e_0 is the initial void ratio; ν_{ur} is the unloading/reloading Poisson's ratio (ν_{ur} is assumed to be 0.2 for clay); $\kappa = C_s/\ln 10$ is the logarithmic swelling index.

For the HSS model, two additional parameters are required in addition to the input parameters of the HS model, such as the reference shear modulus at small strain (G_0^{ref}) and shear strain ($\gamma_{0.7}$) that corresponds to the initial shear modulus equal to $0.7G_0$. In this analysis, two different methods were adopted to determine the reference shear modulus at small strain (G_0^{ref}). The first method was based on the regression line in Fig. 2, where the G_0 values were initially estimated in accordance with the mean effective stress of each soil layer. In order to be used as an input parameter in the HSS model, G_0 values should be further converted to the G_0^{ref} value (*i.e.,* reference shear modulus corresponding to the reference pressure, p^{ref} = 100 kPa). The G_0^{ref} value can be defined by using Eq. (7) (Schanz *et al.* 1999). The second method to determine G_0^{ref} values was based on the empirical formula suggested by Hardin and Black (1969), as described in Eq. (3).

$$G_0 = G_0^{ref} \left(\frac{c \times \cos\phi - \sigma'_3 \sin\phi}{c \times \cos\phi + p^{ref} \sin\phi} \right)^m \tag{7}$$

where c is the soil cohesion; and ϕ is the internal friction angle of soil.

In this analysis, the $\gamma_{0.7}$ value was ranged by $5 \times 10^{-5} \sim 1 \times 10^{-4}$. This range value was assumed based on the typical shear strain for the hypothetical excavation case, which was also verified through case histories (Tseng 2012; Lim and Ou 2017). Besides, the value of $\gamma_{0.7} \le 1 \times 10^{-4}$ usually within the category of small strain, which could reasonably be adopted in the HSS model. The reduction of shear modulus (G) varied by different $\gamma_{0.7}$ values is plotted in Fig. 3. As shown in the figure, the decay of shear modulus was changed for different $\gamma_{0.7}$ values, where the decay rate of shear modulus increased for smaller $\gamma_{0.7}$ values.

For normally consolidated clay, the coefficient of the earth pressure at rest (K_0^{NC}) was determined by using Eq. (8), as suggested by Jaky (1944). Moreover, the over-consolidation ratio (OCR) value could also be taken into consideration to determine K_0^{OC} value, which is automatically calculated in the HS and HSS model by using Eq. (9).

$$K_0^{NC} = 1 - \sin(\phi) \tag{8}$$

$$K_0^{OC} = K_0^{NC} \times \text{OCR} - \frac{\nu_{ur}}{1-\nu_{ur}} (\text{OCR} - 1) \tag{9}$$

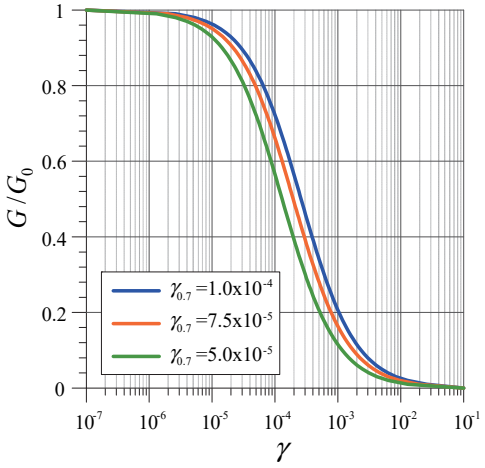

Fig. 3 The difference of shear strain decay rate under the same shear modulus ratio

3.2 Finite Element Modeling

The retaining system, construction sequence, and basic soil properties were assumed to be similar to that of the Taipei National Enterprise Center (TNEC) excavation case (Ou *et al.* 2000). The excavation depth is 19.7 m and is retained by the diaphragm walls with the thickness of 0.9 m and depth of 35 m. The soil was simplified to be a single clay layer, while the soil parameters were followed by the typical clay properties for the TNEC excavation case (Lim 2018). The excavation width (B) was assumed to be 40 m, whereas total clay thickness (H) was assumed to be 40 m and 80 m. The horizontal boundary was extended to be 100 m far from the excavation zone. The retaining system, soil parameters, and construction sequence of the excavation are shown in Fig. 4.

The diaphragm walls (DW) were modeled by the plate elements, while the steel strut and floor slabs (FS) were modeled by the fixed-end anchor. The thickness of DW and FS was set to be 0.9 m and 0.15 m, respectively. Two temporary steel struts were installed at GL −2.3 m and −16.5 m, as detailed in Fig. 4. The concrete compressive strength (f_c') of the DW and FS were assumed to be 27.5 MPa and 20.6 MPa, respectively. The nominal value of

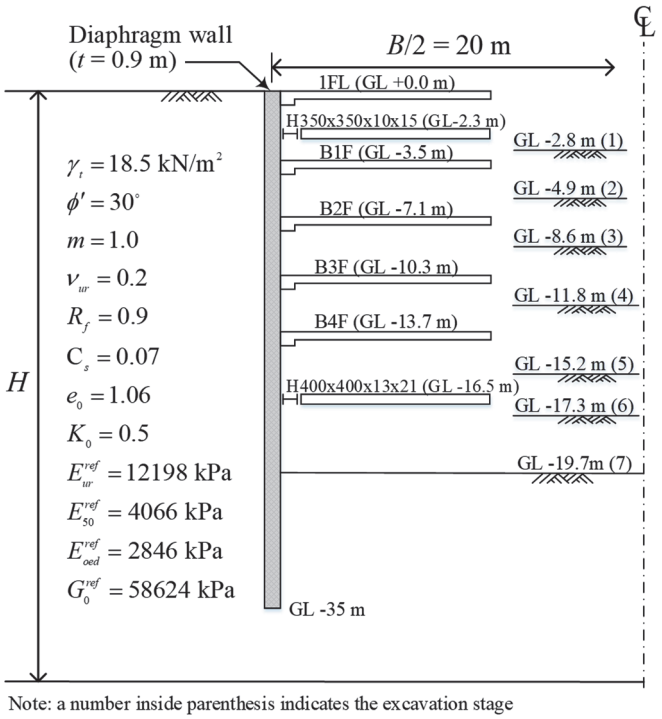

Fig. 4 Profile of subsurface soils and excavation sequence used for the parametric case

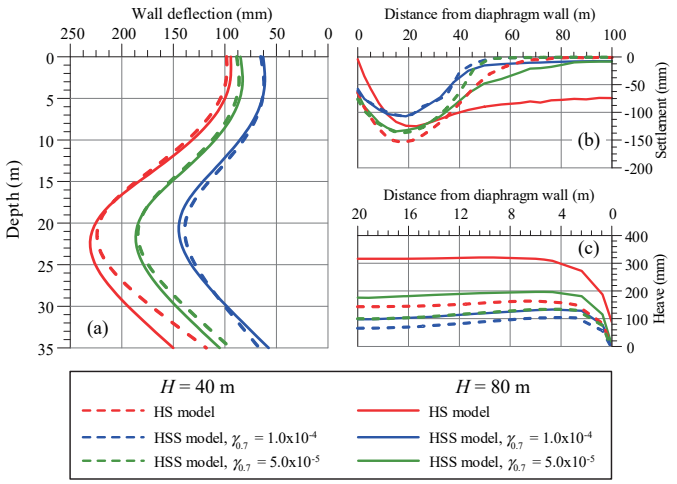

Fig. 5 Finite element results for different $\gamma_{0.7}$ values (C_s = 0.07): (a) computed wall displacement; (b) computed ground settlement; (c) computed soil heave

Young's modulus for concrete material was determined by $E = 4700\sqrt{f_c'}$ [MPa] (ACI 1995). On the other hand, Young's modulus of the steel strut was assumed to be 2.1×10^8 kPa. The structural stiffness of DW, FS, and strut was reduced by 20% to consider the crack in the concrete caused by a large bending moment in the wall and improper installation of the steel strut (Do *et al.* 2016; Lim *et al.* 2016, 2020; Abdi and Ou 2022).

The interaction behavior between the wall and the surrounding soil was modeled as an interface element. The elastic-plastic Coulomb criterion is adopted for the interface element strength to distinguish between elastic behavior (where a small displacement could occur on the interface) and plastic behavior (where permanent slip may occur). Furthermore, the roughness of the interface element is controlled by the strength reduction factor (R_{inter}). When the R_{inter} value is 1.0, the interface strength is the same as that of the surrounding soil, whereas a very low R_{inter} value would result in gaps between the soil and the structure and further increase the relative displacement (Hsieh and Ou 2018; Abdi and Ou 2023). In this study, the R_{inter} value is set to be 0.67, following the typical interface friction between the concrete wall and soil (Ou 2006).

3.3 Finite Element Results

Figures 5(a), 5(b), and 5(c) show the computed wall displacement, ground settlement behind the wall, and soil heave inside the excavation varied by shear strain at $0.7G_0$ ($\gamma_{0.7}$) and soil thicknesses (H = 40-80 m). For the case with H = 40 m, the results showed that the HS model yielded larger computed wall displacement than that of the HSS model, where the wall displacement for the HSS model was reduced along the depth as the $\gamma_{0.7}$ values increased. Similarly, the computed ground settlement and soil heave were also dependent on the $\gamma_{0.7}$ values. This is because the decay rate of shear modulus increased for smaller $\gamma_{0.7}$ values, so the small strain area around the excavation zone decreased, resulting in a larger ground movement. On the other hand, the HS model did not take into consideration the high stiffness at a small strain level, so the ground movement around the excavation was larger than the HSS model. This phenomenon can also be identified by the results of ground settlement, where the HS model would overestimate the location of SIZ compared to that of the HSS model.

For the case with H = 80 m, the computed wall displacement for the HSS model was generally similar to that of H = 40 m, but the wall was kicked out for the HS model. This is because a very large heave occurred inside the excavation, while the computed ground settlement exhibits a very large SIZ area behind the wall. As shown in Figs. 5(b) and 5(c), the results difference between HS and HSS models become more pronounced for a thicker soil (H = 80 m). This indicates that the HS model may overestimate the actual ground movement for a very thick soft clay, so then the HSS model could be considered to provide a more accurate ground movement.

In order to clarify the above findings, the shear modulus ratio (G/G_{ur}) around the excavation zone for different $\gamma_{0.7}$ and H was introduced, as shown in Figs. 6(a), 6(b), 6(c), and 6(d). Note that the stiffness degradation due to plastic straining in the HS small model is simulated with strain hardening. Hence, the small strain stiffness reduction curve is therefore bound by a certain lower limit, where the unloading reloading stiffness, G_{ur} is adopted as the lower cut-off of the shear modulus. The lower cut-off of the shear modulus (G) is introduced at the unloading reloading stiffness (G_{ur}), which is defined by the material parameters E_{ur} and ν_{ur}:

$$G_{ur} = \frac{E_{ur}}{2(1+\nu_{ur})} \tag{10}$$

The cut-off shear strain ($\gamma_{cut\text{-}off}$) at lower limit of shear modulus can be calculated as:

$$\gamma_{cut\text{-}off} = \frac{1}{0.385}\left(\sqrt{\frac{G_0}{G_{ur}}} - 1\right)\gamma_{0.7} \tag{11}$$

According to the above description, the shear modulus ratio (G/G_{ur}) tends to decrease for higher shear strain, whereas the lower shear modulus limited by the unloading-reloading stiffness ($G \geq G_{ur}$). In such a case, a large ground movement area was indicated by a lower G/G_{ur}, and vice versa.

As shown in Figs. 6(a), 6(b), 6(c), and 6(d), it can be seen that a large ground movement (*i.e.,* large strain area) was established around the excavation zone, which was indicated by $G/G_{ur} = 1.0$ (*i.e.,* higher soil stiffness at small strain was not established in this area). Furthermore, the decay rate of shear modulus increased for smaller $\gamma_{0.7}$ values, so the small strain area around the excavation zone decreased and caused larger ground movement (see Fig. 5). For the case with $H = 40$ m, the ground movement below the excavation level was restrained by the stiff soil (see Figs. 6(a) and 6(b)). This resulted in similar results between the HS and HSS model when the distance between the final excavation level and stiff soil is relatively shallow (see Figs. 5(b) and 5(c)). Meanwhile, an excessive ground movement was established below and behind the wall for a deeper stiff soil (H = 80 m), causing a very large ground settlement behind the wall and soil heave inside the excavation for the HS model (see Fig. 5(c)). In such a case, the HSS model has a more significant influence in reducing excessive ground movement as compared to that of $H = 40$ m.

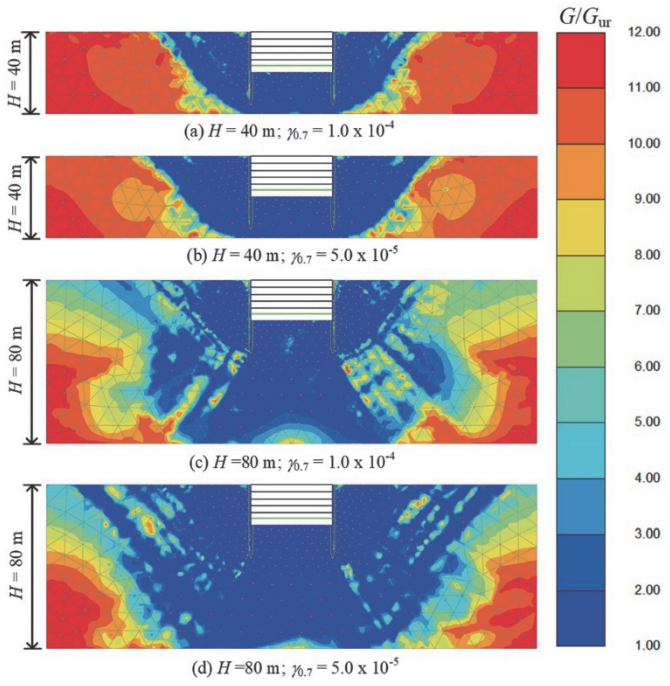

Fig. 6 The distribution of shear modulus ratio (G/G_{ur}) in the soil layer varied by $\gamma_{0.7}$ values (C_s = 0.03): (a) H = 40 m, $\gamma_{0.7}$ = 1.0×10^{-4}; (b) H = 40 m, $\gamma_{0.7}$ = 5.0×10^{-5}; (c) H = 80 m, $\gamma_{0.7}$ = 1.0×10^{-4}; (d) H = 80 m, $\gamma_{0.7}$ = 5.0×10^{-5}

The above findings clearly emphasized that the application of the HSS model was dependent on the clay thickness, where the ground movement between the HS and HSS model tends to be similar when the distance between the final excavation level and stiff soil is not far. This phenomenon can also be explained by using the bearing capacity method. The large ground movement area herein can be represented by the possible basal heave failure surface (Terzaghi 1943), where the radius of the possible basal heave failure surface to the excavation level is the function of excavation width ($B/\sqrt{2}$). Let D defined as the distance between the excavation level and stiff soil. Therefore, for the case with H = 40 m (D = 20.3 m < $B/\sqrt{2}$ = 28.3 m), the results for HS and HSS models tend to be similar because the ground movement below the excavation level is restrained by the stiff soil. On the other hand, the ground movement is not restricted when D = 60 m > $B/\sqrt{2}$ = 28.3 m for the case with H = 80 m, resulting in a more significant influence of the HSS model in reducing the ground movement. Finally, these aspects should be highlighted when considering HS and HSS models in the analysis.

4. CASE VERIFICATION

4.1 TNEC Excavation Case

The Taipei National Enterprise Center (TNEC) is a project with an 18-story structure and a 5-level basement, which is located in Taipei city, Taiwan. The top-down method was adopted for the excavation procedure, while the excavation plan was similar to the trapezoidal with 60 m and 105 m in length and 43 m in width. Note that the retaining system and excavation procedure are the same as that of the parametric case (see Fig. 4). According to the soil investigation report, the soil condition in the TNEC case generally consists of silty clay (CL) and silty sandy soil (SM), where the soil layer can be divided into six main layers based on the soil characteristics (Sungshan I-VI). The detail of soil properties, field monitoring, and excavation plan can be referred to the previous studies (Ou *et al.* 2000; Lim *et al.* 2010). Thus, only a brief summary is presented in this section. In addition, the groundwater table was located at GL –2.0 m (Ou 2006).

The input soil parameters used for analysis are summarized in Table 1. The thick clay layer (Sungshan IV) was divided into

Table 1 Basic soil properties and input soil parameters for TNEC excavation case

Depth (m)	Soil type	γ_t (kN/m^3)	N_{SPT}	OCR	e_0	C_s	c'	ϕ'	ψ	E_{ur}^{ref} (kPa)	E_{50}^{ref} (kPa)	E_{oed}^{ref} (kPa)	$G_0^{ref(a)}$ (kPa)	$G_0^{ref(b)}$ (kPa)
0-2.8	CL	18.25	–	3.25	0.68	0.03	0	30	0	23,214	7,738	5,417	66,237	103,009
2.8-5.6		18.25	–	3	0.75	0.03	0	30	0	22,670	7,557	5,290	53,682	92,936
5.6-8	SM	18.93	6	1	0.82	–	0	31	1	29,121	9,707	9,707	–	–
8-33	CL	18.15	–	1.13-1.48	0.81-1.07	0.032-0.036	0	29	0	19,281-22,622	6,427-7,541	4,499-5,278	43,715-54,882	57,511-86,330
33-35	SM	19.62	23	1	0.76	–	0	31	1	41,014	13,671	1,3671	–	–
35-37.5	CL	19.13	–	1.24	0.7	0.03	0	29	0	23,491	7,830	5,481	46,966	100,027
37.5-41.5	SM	19.62	27	1	0.68	–	0	32	2	55,105	18,368	18,368	–	–
41.5-46		19.62	34	1	0.68	–	0	32	2	66,443	22,148	22,148	–	–

Note: p^{ref} = 100 kPa and v_{ur} = 0.2 for all types of soil; m = 0.5 for CL; m = 1.0 for SM
$G_0^{ref(a)}$ determined based on Teng (2010); $G_0^{ref(b)}$ determined based on Hardin and Black (1969)

many layers because the initial void ratio (e_0) was varied by depth. The stiffness parameters of HS and HSS (E_{ur}^{ref}, E_{50}^{ref}, E_{oed}^{ref}, G_0^{ref}, $\gamma_{0.7}$) were estimated based on the formulas described in the preceding section. Because no test data was provided to determine the small strain shear modulus of sandy soil, the sand layer was simulated using the HS model in this case. Besides, the soil profile mostly consists of the clay layer, so the application of the small strain parameters is only focused on the soft clay layer. Moreover, the structural model and parameters were the same as those in the parametric case.

Due to symmetric, only half of the geometry was modeled in the analysis, as shown in Fig. 7. The horizontal boundary was extended far behind the wall by about four times the excavation depth ($4H_e$) to minimize the boundary restrain. The bottom boundary was set to be at GL −46.0 m to represent the hard stratum level (gravel layer). Furthermore, the horizontal boundaries were constrained from the horizontal movement (roller boundary), while the bottom boundary was restrained in all directions (fixed boundary). In addition, a very fine mesh with local refinement in the interesting area was adopted to provide accurate numerical solutions.

Figures 8(a), 8(b), and 8(c) show the comparison of field measurements and computed wall displacement, ground settlement, and soil heave at the final stage for the TNEC excavation case. The results showed that the computed wall displacement and ground settlement are generally in good agreement with the field measurement, where all results exhibit a concave shape of ground settlement. However, the computed maximum wall displacement (δ_{hm}) for the HS model slightly overestimates the field measurement. For the case with the HSS model, the computed δ_{hm} value was further decreased either by increasing G_0^{ref} or $\gamma_{0.7}$ values. In this case, the HSS model with $\gamma_{0.7} = 5.0 \times 10^{-5}$ (G_0^{ref} determined based on Teng 2010) performs well in predicting the δ_{hm} value from the field measurement. On the other hand, the results from the HSS model with G_0^{ref} determined based on Hardin & Black (1969) slightly underestimate the field measurement. This implies that the empirical formula from Hardin & Black may overestimate the shear modulus at a small strain level in this case, while the shear modulus obtained based on Teng (2010) is suitable to be adopted for the typical excavation case in Taipei. Nevertheless, the G_0^{ref} determined based on Hardin and Black (1969) and Teng (2010) generally exhibited similar results, implying that the empirical method by Hardin and Black (1969) could still be considered in the small strain stiffness model if no experimental test is provided

Moreover, the maximum computed ground settlement (δ_{vm}) for the HS and HSS model (G_0^{ref} referred to Teng 2010; $\gamma_{0.7} = 5.0 \times 10^{-5}$) was close to that of field measurement (see Fig. 8(b)). However, the results for the HS model overestimated the location of SIZ from the field measurement. Meanwhile, the location of SIZ was getting closer to the field measurement for the HSS model with higher G_0^{ref} and $\gamma_{0.7}$ values. Besides, these results are consistent with the findings from the previous studies (Lim *et al.* 2010; Lim and Ou 2017), where the HS model could overestimate the ground settlement behind the wall. Additionally, the results for the HS and HSS model (G_0^{ref} referred to Teng 2010; $\gamma_{0.7} = 5.0 \times 10^{-5}$) were close to each other, implying that the HSS model has an insignificant influence in reducing ground movement. This is because the distance between the excavation level and stiff soil is relatively near (*i.e.*, $D = 13.3\text{ m} < B/\sqrt{2} = 30.4\text{ m}$), so the ground movement below the excavation level is restrained by the stiff soil. Besides, these results are consistent with the finding in the preceding section, where the application of the HSS model is influenced by the distance of the excavation base to the stiff soil (D). Moreover, the computed soil heave showed that the results from the HS model yielded the greatest soil heave, whereas the adoption of HS small strain parameters (G_0^{ref} referred to Teng 2010 and Hardin & Black 1969) would reduce the excessive soil heave inside the excavation (see Fig. 8(c)).

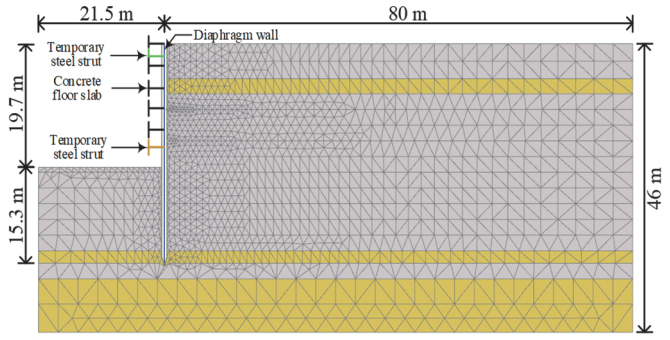

Fig. 7 Finite element used for the TNEC excavation case

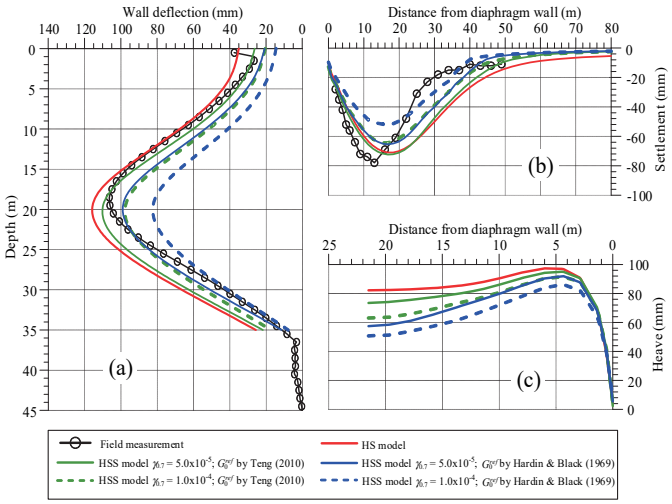

Fig. 8 Comparison of field measurements and finite element results for the TNEC excavation case: (a) wall displacement; (b) ground settlement; (c) soil heave

4.2 Taipei Gas Company Case

The Taipei Gas Company is a project with an 8-story structure and a 4-level basement, which is located in Taipei city, Taiwan. The excavation depth was 18.1 m and supported by the diaphragm wall with 1.0 m in thickness and 40 m in depth. It was braced with the 6-level of steel strut with an average horizontal spacing of 8 m. The excavation plan was similar to the trapezoidal, with 70 m and 87 m in length and 36 m in width. The excavation profile and construction sequence are shown in Fig. 9. In fact, the soil condition in Taipei Gas Company is typically similar to that of the TNEC case because their location is close to each other. A detailed discussion on the soil condition and monitoring data can be referred to in the previous study (Kung *et al.* 2007). Additionally, the groundwater table was located at GL −2.0 m.

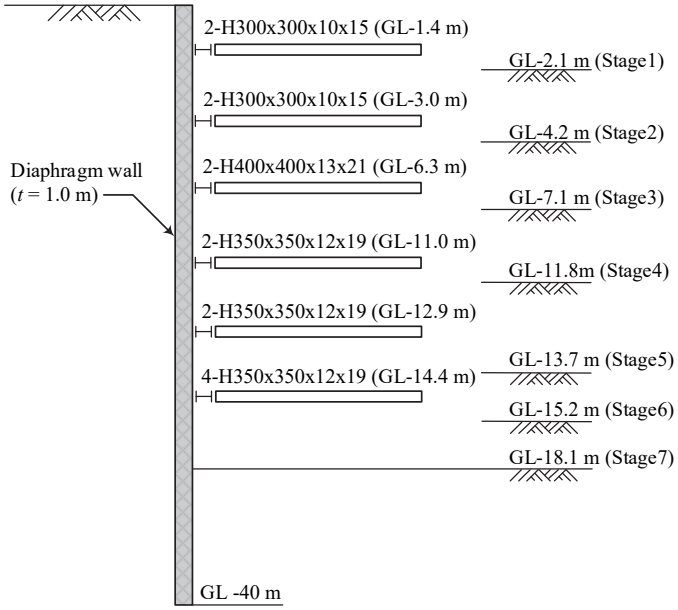

Fig. 9 Profile of subsurface soils and excavation sequence of the Taipei Gas Company excavation case

The finite element mesh, structural model, and determination of structural and soil parameters are the same as those described in the preceding section. In this case, the concrete compressive strength (f_c') of the diaphragm wall was 27.5 MPa. The soil properties and parameters used in this analysis are summarized in Table 2. It can be seen that the basic soil properties adopted in the analysis were typically similar to that of the TNEC case. However, the clay layer (GL –8 m to –42.1 m) for Taipei Gas Company case is relatively thicker than that of the TNEC case. Thus, the diaphragm walls penetrated deeper than those in the TNEC case. Furthermore, the hard stratum (gravel layer) was found below GL –49 m, which was modeled as the bottom boundary (fixed boundary) in the finite element model.

Figures 10(a), 10(b), and 10(c) show the comparison of field measurements and computed wall displacement, ground settlement, and soil heave at the final stage for the Taipei Gas Company excavation case. The results showed that the computed maximum wall displacement (δ_{hm}) from the HS model slightly overestimates the field measurement, whereas the δ_{hm} values from the HSS model (G_0^{ref} based on Teng 2010) were closer to that of field measurement. However, their results were generally similar because the ground movement below the excavation level was restricted by the stiff soil ($D = 24$ m $< B/\sqrt{2} = 25.5$ m), which was similar to that of the TNEC excavation case. Furthermore, the computed wall displacement for the HSS model using G_0^{ref} based on Hardin and Black (1969) with $\gamma_{0.7} = 1.0 \times 10^{-4}$ exhibits the smallest wall displacement and underestimates the δ_{hm} values from the field measurement. Nevertheless, the G_0^{ref} determined based on Hardin & Black (1969) and Teng (2010) generally exhibited similar results, so the empirical formula by Hardin and Black (1969) can be used as an alternate method to determine the reasonable G_0^{ref} values in this case. Furthermore, the computed ground settlement and soil heave showed that the results from the HS model exhibited the greatest value, whereas the results from HS small strain model (G_0^{ref} referred to Teng 2010 and Hardin & Black 1969) would reduce the excessive soil heave inside the excavation (see Fig. 10(c)).

4.3 San Francisco Excavation Case

The San Francisco excavation case occupied a plan of 87 m in length and 42.7 m in width, while the excavation depth is 14 m. This project was located in California, USA. In order to support the excavation, the sheet-pile wall (MZ-32) was installed and penetrated until it reached the dense sand level. Three level of steel strut with 5 m in horizontal spacing was adopted as a bracing system. The excavation profile and construction sequence are shown in Fig. 11. Before installing the sheet pile walls, the top of the rubble fill layer was initially removed at about 3.35 m. The top level

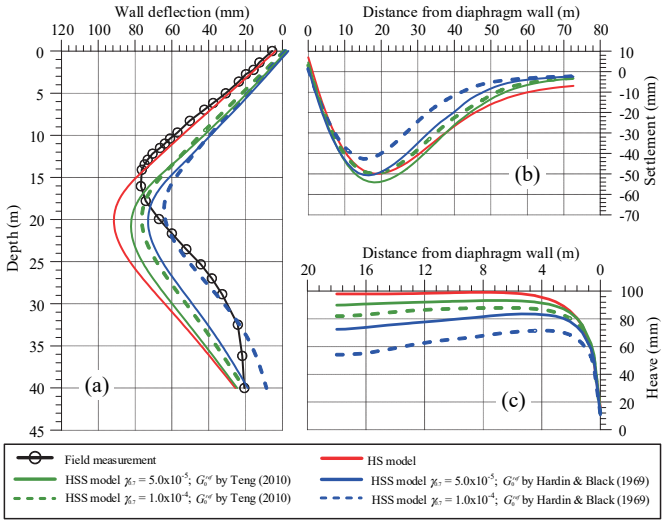

Fig. 10 Comparison of field measurements and finite element results for the Taipei Gas Company excavation case: (a) wall displacement; (b) ground settlement; (c) soil heave

Table 2 Basic soil properties and input soil parameters for Taipei Gas Company excavation case

Depth (m)	Soil type	γ_t (kN/m^3)	N_{SPT}	OCR	e_0	C_s	c'	ϕ'	ψ	E_{ur}^{ref}(kPa)	E_{50}^{ref} (kPa)	E_{oed}^{ref} (kPa)	$G_0^{ref(a)}$ (kPa)	$G_0^{ref(b)}$ (kPa)
0-1.4	Fill	18.25	7	1	0.68	0.03	0	32	2	62,708	20,903	20,903	–	–
1.4-5	CL	18.25	–	3	0.75	0.03	0	30	0	24,182	8,061	5,642	54,459	92,936
5-8.3	SM	18.93	6	1	0.82	–	0	31	1	29,249	9,750	9,750	–	–
8-32.8	CL	18.15	–	1.13-1.48	0.8-1.07	0.032-0.036	0	29	0	21,994-24,484	7,331-8,161	5,132-5,713	43,536-54,147	57,551-86,330
32.8-37.8	CL	19.13	–	1.24	0.7	0.03	0	29	0	23,491	7,830	5,481	41,839	100,027
37.8-42.1	CL	19.13	–	1.24	0.7	0.03	0	29	0	23,491	7,830	5,481	41,558	100,027
42.1-49	SM	19.62	30	1	0.68	–	0	32	2	57,611	19,204	19,204	–	–

Note: $p^{ref} = 100$ kPa and $v_{ur} = 0.2$ for all types of soil; m = 0.5 for CL; m = 1.0 for SM
$G_0^{ref(a)}$ determined based on Teng (2010); $G_0^{ref(b)}$ determined based on Hardin and Black (1969)

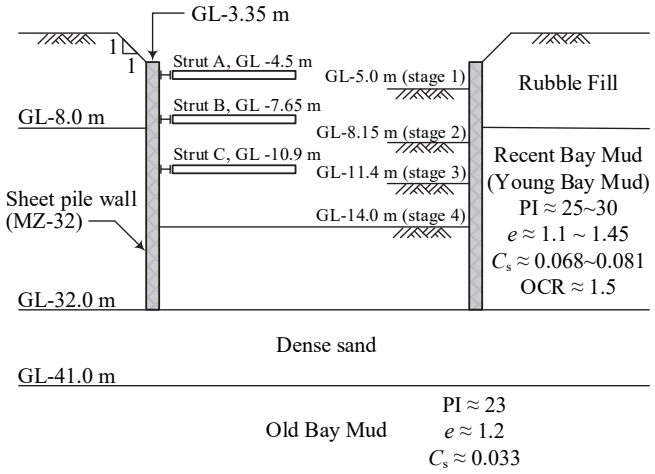

Fig. 11 Profile of subsurface soils and excavation sequence of the San Francisco excavation case

of sheet pile walls was set to be at GL −3.35 m. Moreover, the soil was further excavated until it reached GL −14 m, which was divided into four excavation stages. A detailed discussion on the field instrumentation and monitoring data can be referred to in the previous study (Mana 1980). Moreover, the groundwater table was located at GL −3.4 m.

The soil condition in the San Francisco case mostly consisted of harbor sedimentation with relatively high water content (ω), plasticity index (PI), void ratio (e), and swelling index (C_s), which can be categorized as weak soil. According to Mana (1980), the shallow sediment (referred to as Recent Bay Mud or Young Bay Mud) in this project has a water content and liquid limit of about 60%, while the PI ranges from 25 to 30. Furthermore, the remaining basic soil properties at each layer were determined based on the site investigation reported by FUGRO (2018).

In this case, the shear modulus at small strain (G_0) was determined based on the shear wave velocity (V_s), as measured by Gibbs *et al.* (1994). It was found that the V_s values for the coarse-grained soil (rubber fill and dense sand layer) typically ranged from 260 to 300 m/sec. On the other hand, the V_s values for the Young Bay Mud layer ranged by V_s = 130-170 m/sec, while the Old Bay Mud layer has V_s = 300 m/sec. Furthermore, the determination of G_0 value associated with V_s value can be defined as:

$$G_0 = \rho V_s^2 \quad [\text{MPa}] \tag{12}$$

where ρ is the total density of soil (kg/m^3); and V_s is the shear wave velocity (m/sec). In order to be used as an input parameter in the HSS model, the shear modulus in Eq. (12) should be converted to the G_0^{ref} (reference shear modulus corresponding to the reference pressure, p^{ref} = 100 kPa), as expressed in Eq. (7).

The basic soil properties and input soil parameters are summarized in Table 3. In this analysis, the thick layer of Young Bay Mud was divided into six layers within 4 m intervals. The finite element mesh, structural model, and structural parameters are the same as those described in the preceding section. Note that the sheet pile walls were modeled as plate elements, in which its parameter should be modified based on the bending stiffness (Brinkgreve *et al.* 2013). In addition, the structural parameters in the analysis were adopted based on Mana (1980).

Figures 12(a), 12(b), and 12(c) show the comparison of field measurements and computed wall displacement, ground settlement, and soil heave at the final excavation stage. The results showed that the computed wall displacement for the HS model and finite element results provided by Mana (1980) were typically similar, which overestimated the field measurement. This is due to the fact that those analyses did not take into consideration the higher soil stiffness at a small strain level, so the excessive ground movement behind the wall was established, resulting in a large wall displacement and ground settlement. On the other hand, the adoption of the HSS model could provide more reasonable results, where the computed wall displacement along the depth was reduced and closer to that of field measurement.

As shown in Fig. 12(b), it can be seen that the HSS model with $\gamma_{0.7} = 1.0 \times 10^{-4}$ performed well in predicting the wall displacement, where the computed maximum wall displacement had a close agreement with that of field measurement. In fact, the suitable $\gamma_{0.7}$ value for this case is higher than that of the typical excavation case in Taipei (*i.e.,* the TNEC and Taipei Gas Company case). This is because the soil properties in the San Fransisco case are relatively weak, so a higher $\gamma_{0.7}$ value should be considered in the analysis. Furthermore, the computed wall displacement and ground settlement for HSS were typically similar for different G_0^{ref} values (S-wave velocity and Hardin and Black 1969). It is because the G_0^{ref} values determined by the S-wave velocity had a slight difference from that of Hardin and Black (1969) for the Young Bay Mud layer. Hence, the empirical formula from Hardin and Black (1969) could be considered in this case if no sufficient test data was provided for the small strain shear modulus. Additionally, the computed wall displacement and ground settlement for HS and HSS models were generally similar because the ground movement was restrained by the stiff soil ($D = 18$ m $< B/\sqrt{2} = 30.2$ m), which was consistent with the other case studies. Moreover, the computed soil heave showed that the results from the HS model exhibited the greatest soil heave, whereas the results from HS small strain model (G_0^{ref} based on S-Wave velocity and Hardin & Black 1969) would reduce the excessive soil heave inside the excavation (see Fig. 12(c)).

Table 3 Basic soil properties and input soil parameters for San Francisco excavation case

Depth (m)	Soil type	γ_t (kN/m^3)	N_{SPT}	OCR	e_0	C_s	c'	ϕ'	ψ	E_{ur}^{ref} (kPa)	E_{50}^{ref} (kPa)	E_{oed}^{ref} (kPa)	$G_0^{ref(a)}$ (kPa)	$G_0^{ref(b)}$ (kPa)
0-8	Fill	17.27	20	1	0.5	–	0	30	0	106,755	35,585	35,585	–	–
8-32	CL	17.27	–	1.5	1.1-1.45	0.068-0.081	0	28	0	11,246-14,108	3,749-4,703	2,624-3,292	33,461-51,955	31,243-55,128
32-41	SM	18.84	58	1	0.5	–	0	38	8	105,311	35,104	35,104	–	–
41-52	CL	17.66	–	1.5	1.2	0.033	0	28	0	27,631	9,210	6,447	67,484	47,153

Note: p^{ref} = 100 kPa and v_{ur} = 0.2 for all types of soil; m = 0.5 for CL; m = 1.0 for SM

$G_0^{ref(a)}$ determined based on the S-waves velocity; $G_0^{ref(b)}$ determined based on Hardin and Black (1969)

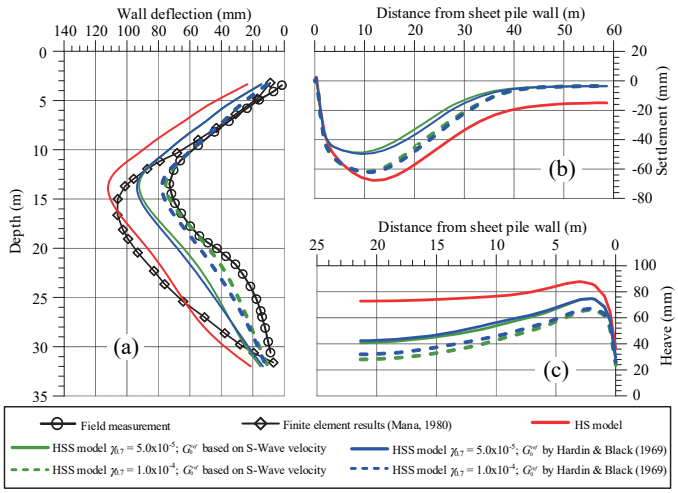

Fig. 12 Comparison of field measurements and finite element results for the San Francisco excavation case: (a) wall displacement; (b) ground settlement; (c) soil heave

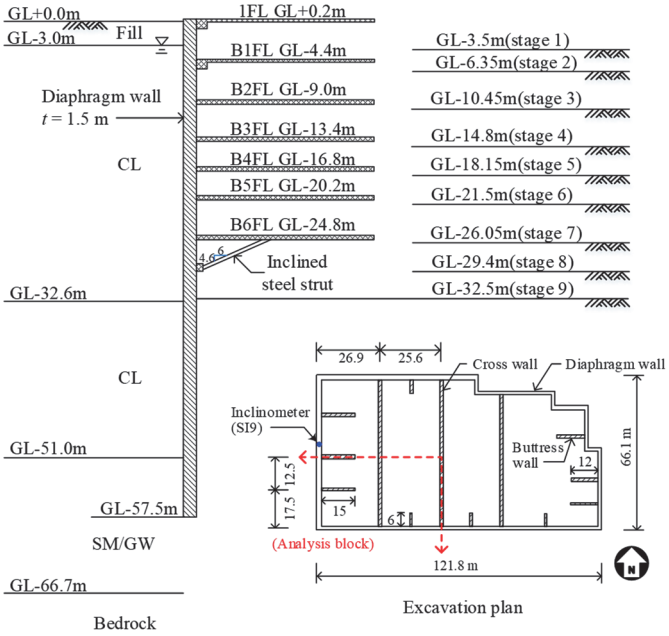

Fig. 13 Profile of subsurface soils, excavation sequence, and excavation plan of the UPIB excavation case

4.4 UPIB Excavation Case

The UPIB excavation case is located in Taipei city and designed with a seven-level basement, which occupied a plan of 121.8 m in length and 66.1 m in width. The excavation depth is 32.5 m and retained by the diaphragm wall with a thickness of 1.5 m and a depth of 57.5 m. The excavation was carried out by adopting the top-down method. The concrete floor slab was installed after excavating the soil, while the temporary inclined steel strut (H400 × 400 × 13 × 21) was used prior to the final excavation stage with an average horizontal spacing of 6.4 m. Concerning the excessive wall displacement and ground settlement during excavation, the buttress and cross wall was implemented directly after the completion of the main diaphragm walls. Figure 13 shows the excavation profile, construction sequence, and excavation plan for the UPIB case. Furthermore, the groundwater table was located -3.0 m below the ground surface.

In this case, the thickness of the concrete floor slab for 1FL is 0.25 m, B1FL is 0.2 m, and the thickness of the remaining floor (B2FL to B6FL) is 0.61 m. On the other hand, the thickness of the buttress and cross wall is 1.0 m. The cross wall was installed from GL −1.5 m to GL −45.0 m (43.5 m), while the buttress wall was implemented from GL −1.5 m to 55.0 m (53.5 m). The compressive strength of the diaphragm walls and concrete floor slab is 26.5 MPa. Note that the buttress and cross walls between GL −1.5 m and GL −22.0 m were cast with 13.7 MPa, and those below GL −22.0 m were cast with 27.5 MPa. It is because the cross and buttress walls were demolished along with the excavation, so no reinforcement steel bars were considered above the final excavation level (*i.e.,* lower compressive strength).

The soil condition for this case was different from that of the TNEC and Taipei Gas Company excavation case, where the soil layer was interbedded with sand and clay. The soil layer mainly consisted of thick silty clay from the ground surface, which is relatively weak. Thus, the diaphragm wall was penetrated until it reached the stiff soil layer (SM/GW), which was found at GL −51.0 m (see Fig. 13). The hard stratum (bedrock layer) was found 66.7 m below the ground surface, in which its N-SPT value is greater than 50.

Basic soil properties and input soil parameters for the UPIB case are summarized in Table 4. A detailed discussion of the soil condition in the UPIB case can be found in the previous study (Ou *et al.* 2006; Hsieh and Ou 2018). In this case, the first and second thick clay layer was divided into many layers. Because this project was located in Taipei, the reference shear modulus at small strain (G_0^{ref}) was determined based on the experimental test (Teng 2010) and the correlation formula (Hardin and Black 1969), which was similar to that of TNEC and Taipei Gas Company excavation case. Furthermore, the nominal value of Young's modulus for concrete material was determined by $E = 4700\sqrt{f_c'}$ [MPa] (ACI 1995), whereas Young's modulus of steel strut was assumed to be 2.1×10^8 kPa. All structural stiffness (diaphragm wall, buttress wall, cross wall, and concrete floor slab) were reduced by 20% to consider the crack in the concrete caused by a large bending moment.

Table 4 Basic soil properties and input soil parameters for UPIB excavation case

Depth (m)	Soil type	γ_t (kN/m^3)	N_{SPT}	OCR	e_0	C_s	c'	ϕ'	ψ	E_{ur}^{ref} (kPa)	E_{50}^{ref} (kPa)	E_{oed}^{ref} (kPa)	$G_0^{ref(a)}$ (kPa)	$G_0^{ref(b)}$ (kPa)
0-8	Fill	18.25	–	4.5	0.97	0.04	0	30	0	20,416	6,805	4,764	76,258	67,206
3-32.6	CL	18.05	–	1.5-1.0	0.8-1.3	0.04-0.05	0	30	0	14,923-23,836	4,974-7,945	3,482-5,562	47,270-72,355	40,159-86,569
32.6-51	CL	18.74	–	1.5	0.6-0.9	0.03-0.045	0	31	1	16,950-22,938	5,650-7,646	3,955-5,352	40,747-41,710	74,638-116,142
51-67	SM/GW	19.62	> 50	1	0.6	–	0	37	7	256,000	85,000	85,000	–	–

Note: p^{ref} = 100 kPa and ν_{ur} = 0.2 for all types of soil; m = 0.5 for CL; m = 1.0 for SM
[a] G_0^{ref} determined based on Teng (2010); [b] G_0^{ref} determined based on Hardin and Black (1969)

Because the buttress wall behavior cannot be determined by the two-dimensional (2D) plane strain analysis, the three-dimensional (3D) finite element analysis was conducted in this case, as shown in Fig. 14. The diaphragm, buttress, cross wall, and concrete floor slab were modeled as plate element, in which their connection was assumed to be fixed (*i.e.,* shares all degrees of freedom). The inclined steel strut was simulated by the beam element. Only a quarter of the excavation geometry (denoted as analysis block in Fig. 13) was considered in the finite element model for simplicity. The horizontal boundary was extended far from the excavation zone by considering the excavation depth ($4H_e$) to minimize the effect of the boundary restrain. The four sides of horizontal boundaries were constrained from the horizontal movement (roller boundary), while the bottom boundary was restrained in all directions (fixed boundary).

Figure 15(a) shows the comparison of field measurement (SI9) and computed wall displacement at the final excavation stage for the UPIB case. It is found that the results from the HS model slightly overestimate the field measurement. Under such a case, the HS and HSS model were generally identical because the ground movement was restrained by the stiff soil ($D = 18.5$ m $< B/\sqrt{2} = 85.9$ m), which was similar to that of the other excavation cases. Furthermore, a close agreement was found between the field measurement and the HSS model ($\gamma_{0.7} = 5.0 \times 10^{-5}$; G_0^{ref} based on Teng 2010). Indeed, this result is consistent with the previous findings, where G_0^{ref} based on Teng (2010) performs well in predicting the wall displacement for the typical excavation case in Taipei clay. Meanwhile, the HSS model based on Hardin and Black (1969) underestimates the maximum wall displacement from the field measurement, implying that the assumption of G_0^{ref} values may be too high. However, the ground settlement results showing that the HSS model based on Hardin and Black (1969) for $\gamma_{0.7} = 1.0 \times 10^{-4}$ had a close agreement to that of field measurement, as shown in Fig. 15(b). Nevertheless, the adoption of HS model in this case could slightly overestimate the field measurement for wall displacement and ground settlement, indicating that the HSS model could performed better in predicting the ground movement and simulating the actual soil behavior ($D = 18.5$ m $< B/\sqrt{2} = 85.9$ m).

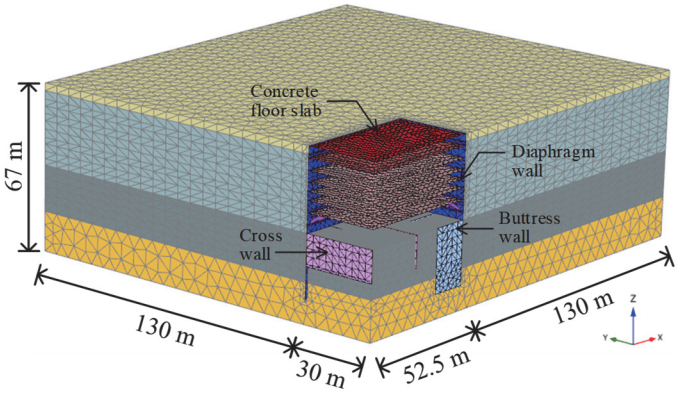

Fig. 14 Finite element mesh and structural model used for UPIB case

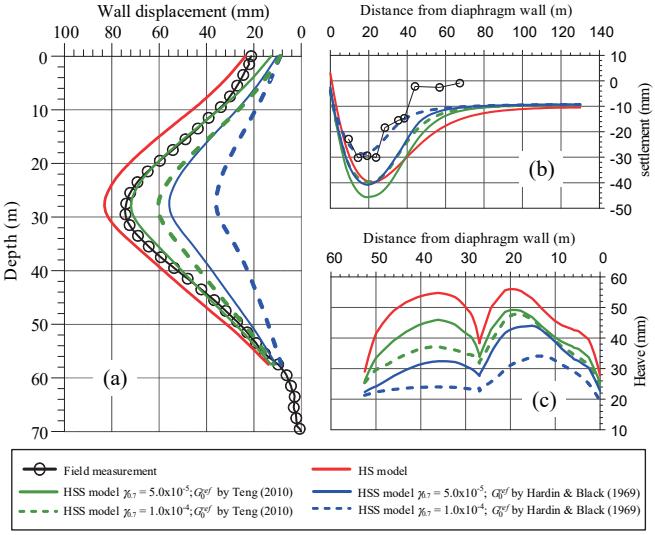

Fig. 15 Comparison of computed wall displacement and computed wall displacement for UPIB excavation case: (a) wall displacement; (b) ground settlement; (c) soil heave

Moreover, the soil heave results inside the excavation showing that the HS model would yielded the greatest heave, while the soil heave would reduce when using HSS model. Besides, the shape of soil heave in this case was different to that of other cases. It is due the existence of cross walls inside the excavation that could resist the soil heave.

4.5 Wenlinyuan Excavation Case

The Wenlinyuan project is a reinforced concrete structure with a fifteen-story structure and a three-level basement located in Shilin District, Taipei city. The excavation plan has a dimension of 47.6 m × 36.9 m, while the excavation depth is 11.9 m. The 0.6 m in thickness and 28 m in depth diaphragm walls were installed to support the excavation. The bottom-up method was adopted for the excavation process, in which four levels of temporary steel struts were implemented along with the excavation. Figures 16(a) and 16(b) shows the detail of the excavation profile, construction procedure, and excavation plan for the Wenlinyuan case. In this case, the barrette piles were implemented and arranged by the cross wall pattern on the west side, whereas the buttress wall pattern was on the east side. The buttress and cross wall thickness was 0.6 m and installed from GL −3 m to GL −25 m (22 m in depth). The buttress and cross wall above the B3F level (GL −9.6 m) was demolished along with excavation. The buttress and cross wall at −3 m to −11.9 were cast by low-strength concrete (13.7 MPa), and those at a level below −11.9 m were cast by reinforced concrete (21 MPa).

Furthermore, the building with four and nine stories structures and a 2-level basement (the depth of the basement and diaphragm wall were 7 m and 13 m, respectively) existed adjacent to the south side of the excavation plan. Two adjacent buildings also existed on the northwest side, which was supported by the raft foundation (see Fig. 16(b)). Therefore, the existence of the adjacent building was considered in the analysis because its distance to the excavation area was relatively near and may affect the wall displacement results.

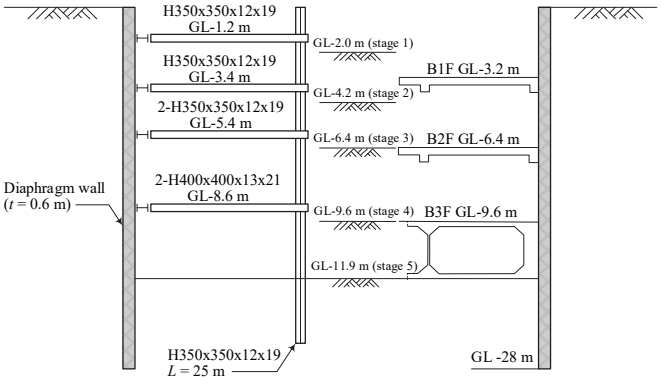

(a) Profile of subsurface soils and excavation sequence

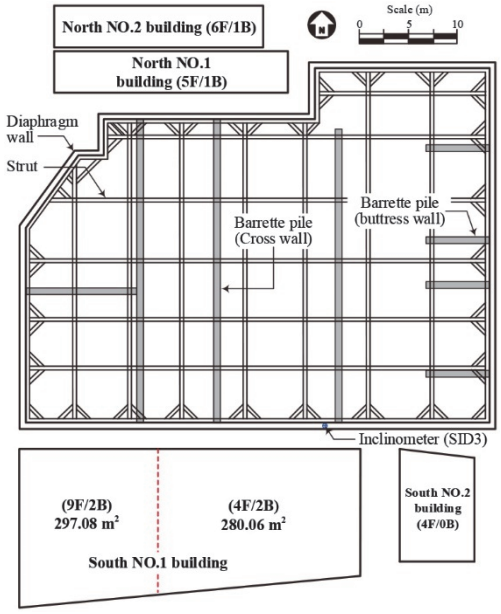

(b) Excavation geometry and instrumentation plan

Fig. 16 Wenlinyuan excavation project

The soil condition for this case was interbedded with the clay and sand layer, where the hard stratum was found at GL –46.5 m. The basic soil properties (SPT-N, OCR, C_c, C_s, and e) at various depths were collected around the site. The soil parameters for HS and HSS models used in the analyses are summarized in Table 5. Note that the C_s value was obtained based on the empirical formula (C_s = PI/370), as suggested by (Kulhawy and Mayne 1990). Moreover, the stiffness parameters (E_{ur}^{ref}, E_{50}^{ref}, E_{oed}^{ref}, G_0^{ref}) were calculated based on Eqs. (4) to (7).

In accordance with the stiffness parameter obtained from the empirical formula (C_s = PI/370), the soil test (oedometer test) was also performed through the finite element method to estimate the optimization of soil stiffness parameters. Figure 17 shows the unloading-reloading soil stiffness (E_{ur}) based on the empirical formula and the optimization analysis (soil test). It can be seen that the E_{ur} value for different methods was generally similar. This indicates that the stiffness parameter determined by the empirical formula could be reasonably used for the analysis.

Three-dimensional finite element analysis was used to conduct the Wenlinyuan excavation case, which was similar to that of the UPIB case. However, a full excavation geometry was modeled in the analysis to consider the existence of an adjacent building. Figure 18(a) shows the finite element used for the Wenlinyuan excavation case. The horizontal boundary was extended about four times the excavation depth ($4H_e$), while the bottom boundary was set to be at GL –46.5 m. Furthermore, the detail of the structural model used in the analysis is shown in Fig. 18(b). The steel strut and center post were simulated by the beam element, whereas the diaphragm wall was modeled by the plate element. In addition, the retaining system of the adjacent building (diaphragm wall and floor slab) was also modeled by the plate element.

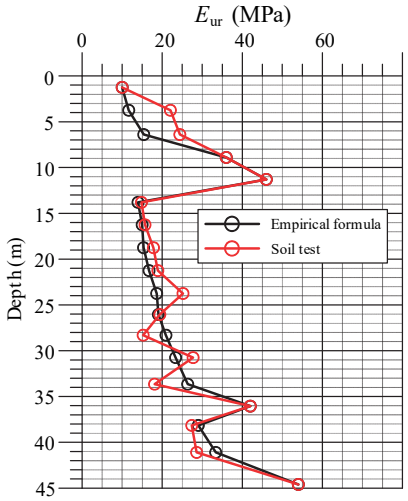

Fig. 17 Different methods to determine the input parameters of the unloading-reloading soil stiffness (E_{ur})

Table 5 Basic soil properties and input soil parameters for Wenlinyuan excavation case

Depth (m)	Soil type	γ_t (kN/m^3)	N_{SPT}	OCR	e_0	C_s	c'	ϕ'	ψ	E_{ur}^{ref} (kPa)	E_{50}^{ref} (kPa)	E_{oed}^{ref} (kPa)	$G_0^{ref(a)}$ (kPa)	$G_0^{ref(b)}$ (kPa)
0-2.5	SF	18.84	5	1	0.8	–	0	27	0	27,887	9,296	9,296	–	–
2.5-7.8	CL	17.66	–	1.75-1.9	0.94-1.04	0.031-0.032	0	26	0	25,938-26,422	8,646-8,807	6,052-6,165	53,462-56,933	60,256-70,098
7.8-12.6	SM	18.76	18 ~ 23	1	0.75-0.85	–	0	31	1	50,809-59,081	16,936-19,694	16,936-19,694	–	–
12.6-35.3	CL	18.02-18.41	–	1.05-1.2	0.9-1.06	0.05-0.06	0	27-29	0	13,954-16,164	4,651-5,388	3,256-3,772	42402-50,491	54,951-74,422
35.3-36.8	SM	19.33	21	1	0.73	–	0	32	2	33,607	11,202	11,202	–	–
36.8-42.7	CL	19.16	–	1.2	0.78-0.82	0.047-0.049	0	30	0	15,056-16,050	5,019-5,350	3,513-3,745	42,437-42,447	83,815-88,916
42.7-46.5	ML/SM	18.92	27	1	0.79	–	0	31	1	38,233	12,744	12,744	–	–

Note: p^{ref} = 100 kPa and v_{ur} = 0.2 for all types of soil; m = 0.5 for CL; m = 1.0 for SM
$G_0^{ref(a)}$ determined based on Teng (2010); $G_0^{ref(b)}$ determined based on Hardin and Black (1969)

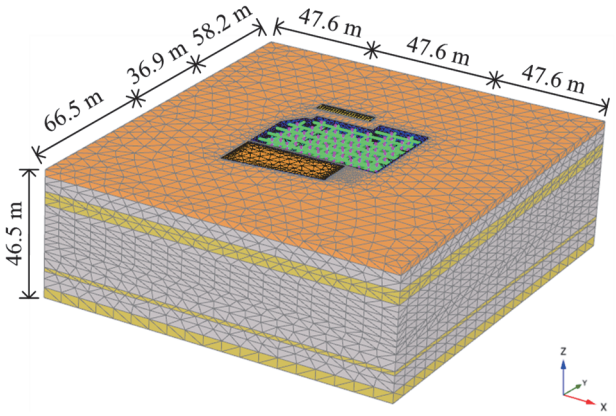

(a) Finite element used for analysis

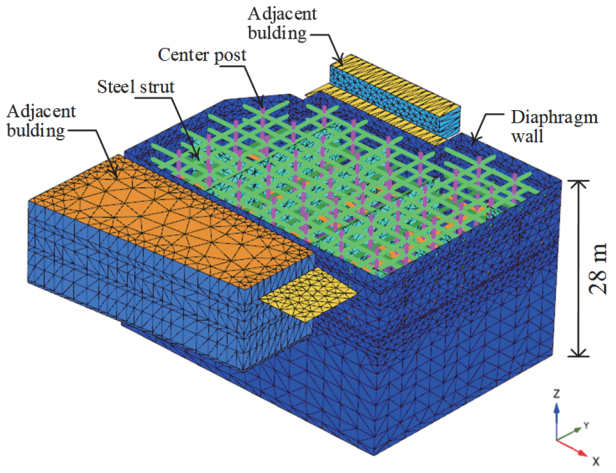

(b) Detail of the structural model

Fig. 18 The finite element model of Wenlinyuan excavation project

Figure 19(a) presents the computed soil heave inside the excavation. As shown in the figure, the existence of center posts inside the excavation could resist the soil heave. Furthermore, the HS model yielded the greatest results, while the heave would significantly reduce as the HSS model was adopted. This is because the distance between the excavation base to the stiff soil is relatively far ($D = 23.4$ m $> B/\sqrt{2} = 22.3$ m), so the adoption of HSS model has significant influence to the ground movement. Indeed, this phenomenon is in agreement to that of the finding in the parametric studies, where the results difference between HS and HSS model would be more pronounced for a thicker clay layer.

Figure 19(b) shows the comparison of field measurement and computed wall displacement at the final excavation stage. The results from the HS model showed that the wall toe was kicked out, resulting in an overestimation of wall displacement from the field measurement. The reason is that the diaphragm wall was not penetrated into the stiff soil layer, while the stiff soil was located far below the excavation level ($D = 23.4$ m $> B/\sqrt{2} = 22.3$ m). Thus, a very large ground movement was developed, resulting in an excessive soil heave inside the excavation, causing the wall toe to kick out. Under such conditions, the HSS model could be considered to reduce the excessive ground movement around the excavation zone significantly.

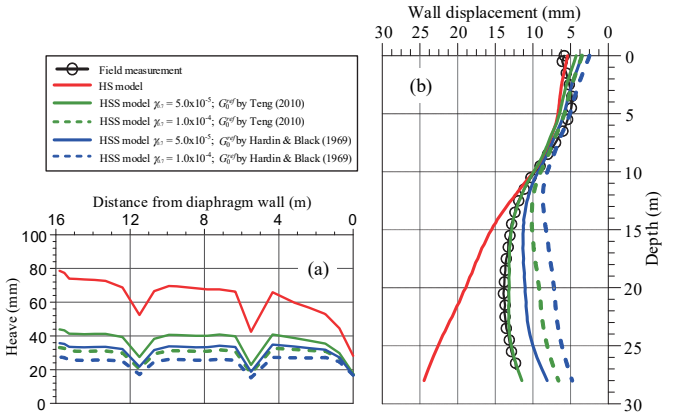

Fig. 19 Comparison of computed wall displacement and computed wall displacement for Wenlinyuan excavation case: (a) soil heave; (b) wall displacement

As shown in Fig. 19(b), the computed wall displacement below the final excavation level was significantly reduced for the HSS model with higher G_0^{ref} and $\gamma_{0.7}$ values. It is found that the results from the HSS model ($\gamma_{0.7} = 5.0 \times 10^{-5}$; G_0^{ref} based on Teng, 2010) perfectly fit the field measurement in this case. Meanwhile, the computed wall displacement for the HSS model based on Hardin & Black (1969) slightly underestimate the field measurement below the final excavation level. Nevertheless, those methods generally exhibited identical results, which was consistent with the findings in other excavation cases. Additionally, these findings further confirm that the application HSS model in a very thick clay layer ($D \geq B/\sqrt{2}$) has a significant influence in reducing the ground movement, which could provide more accurate results in predicting wall displacement.

5. DISCUSSION

According to the findings in the parametric case, the influence of the HSS model in reducing ground movement was affected by the distance (D) between the excavation level and stiff soil. In such a case, the results for HS and HSS models would be identical when $D < B/\sqrt{2}$ because the ground movement below the excavation level was restricted by the stiff soil. Meanwhile, the influence of the HSS model in reducing the ground movement becomes more pronounced for the case with $D \geq B/\sqrt{2}$. Besides, these findings were confirmed by the analysis results in the case studies. Take an example for the Wenlinyuan case ($D \geq B/\sqrt{2}$), the computed wall displacement for the HSS model was much smaller than that of the HS model, in which the results for the HSS model had a close agreement to that of field measurement. Hence, the distance of excavation base to the stiff soil should be highlighted when considering the HSS model in the analysis.

Based on the analysis results for the several case histories, the relationship between the swelling index (C_s), shear strain ($\gamma_{0.7}$), and the construction method can be summarized in Table 6. It indicates that a smaller $\gamma_{0.7}$ value can be considered in the analysis for the top-down method with relatively weak soil. This is because the top-down method usually has a longer construction time, which may induce soil creep and cause a large ground movement around

the excavation area. Under such conditions, a smaller $\gamma_{0.7}$ value ($\gamma_{0.7} = 5 \times 10^{-5}$) for the HSS model could perform well in predicting the wall displacement induced by deep excavation (*e.g.,* TNEC and UPIB cases). On the other hand, a larger $\gamma_{0.7}$ value ($\gamma_{0.7} = 1 \times 10^{4}$) would exhibit the over-conservative results, where the computed wall displacement was smaller than the field measurement.

Furthermore, the creep effect for the bottom-up method is relatively small during construction, so then a larger $\gamma_{0.7}$ value ($\gamma_{0.7} = 1 \times 10^{-4}$) can be used in the analysis (*e.g.,* Taipei Gas Company and San Francisco cases). For the Wenlinyuan case, the $\gamma_{0.7}$ value can be selected by the typical range ($\gamma_{0.7} = 5 \times 10^{-5} \sim 1 \times 10^{-4}$), but $\gamma_{0.7} = 5 \times 10^{-5}$ is preferred. The reason is that the distance between the excavation level and stiff soil is very deep ($D \geq B/\sqrt{2}$), so a smaller $\gamma_{0.7}$ value can be considered in the analysis.

Table 6 The relationship between shear strain ($\gamma_{0.7}$), swelling index (C_s), and construction method for several case histories

Excavation case	C_s	$\gamma_{0.7}$	Construction method
TNEC	0.03-0.04	5×10^{-5}	Top-down method (creep effect)
Taipei gas company	0.03-0.04	1×10^{-4}	Bottom-up method
San Francisco	0.07-0.08	1×10^{-4}	Bottom-up method
UPIB	0.03-0.05	5×10^{-5}	Top-down method (creep effect)
Wenlinyuan	0.05-0.06	5×10^{-5} - 1×10^{-4}	Bottom-up method

6. CONCLUSIONS

A series of finite element analyses were conducted to evaluate the influence of small strain parameters in deep excavation problems. Two advanced soil models, such as hardening soil (HS) and hardening soil with small strain (HSS), were adopted in this study. Several case histories (TNEC case, Taipei Gas Company case, San Francisco case, UPIB case, and Wenlinyuan case) were also considered to verify the analysis method. Based on the findings in this paper, the following conclusion can be drawn:

1. When the stiff soil is located near the excavation level ($D < B/\sqrt{2}$), the results for HS and HSS models are similar. It is because the ground movement below the excavation level was restrained by the stiff soil. However, if the soil condition is relatively weak and the stiff soil is located far below the excavation level (*i.e.,* $D \geq B/\sqrt{2}$), the results for HS and HSS models will be different. In that case, the HSS model should be used to present accurate ground movement and predict the field measurement well. On the contrary, the HS model would overestimate the field measurement because it did not consider the higher soil stiffness at small strain.
2. According to the analysis results, the reference shear modulus at small strain (G_0^{ref}) obtained by the experimental test (*e.g.,* bender element tests and in-situ shear wave velocity tests) and the empirical formula (Hardin and Black 1969) generally exhibited similar analysis results. Hence, the empirical formula from Hardin and Black (1969) could be reasonably adopted as a preliminary approach to determine the small strain shear modulus if no sufficient test data is provided.
3. According to the analysis results from several case histories, the small strain parameter ($\gamma_{0.7}$) has a relationship with the construction method and swelling index (C_s). The soil creeps effect is usually found in the excavation case with the top-down method in soft clay, which could induce excessive ground movement. Under such conditions, a smaller $\gamma_{0.7}$ value ($\gamma_{0.7} = 5 \times 10^{-5}$) can be considered for the HSS model. On the other hand, the creep effect is relatively small for the excavation with the bottom-up method, in which a larger $\gamma_{0.7}$ value ($\gamma_{0.7} = 1 \times 10^{-4}$) can be used to simulate the small strain behavior in the deep excavation problem. In addition, the creep effect is usually large for the relatively weak soil (higher C_s), so a smaller $\gamma_{0.7}$ value ($\gamma_{0.7} = 5 \times 10^{-5}$) can be used in the analysis.

ACKNOWLEDGEMENT

The authors would like to thank the CECI Engineering Consultants, Taiwan for their support. These supports made this study and further research possible.

DATA AVAILABILITY STATEMENT

All data, models, and code generated or used during the study appear in the submitted article.

CONFLICT OF INTEREST

The author(s) declare(s) that there is no conflict of interest.

REFERENCES

Abdi, A.S. and Ou, C.Y. (2022). "A study of the failure mechanism of braced excavations using 3D finite-element analysis." *International Journal of Geomechanics*, ASCE, **22**(7), 1-14. https://doi.org/10.1061/(ASCE)GM.1943-5622.0002385

Abdi, A.S. and Ou, C.Y. (2023). "Numerical study of the effect of ground improvement on basal heave stability for deep excavations in normally consolidated clays." *Journal of Geotechnical and Geoenvironmental Engineering*, **149**(7), 1-11. https://doi.org/10.1061/JGGEFK.GTENG-11022

ACI, Committee. (1995). *Building Code Requirements for Structural Concrete*, Farmington Hills: ACI 318R-American Concrete Institute.

Benz, T. (2007). *Small-Strain Stiffness of Soils and Its Numerical Consequences.* University of Stuttgart.

Brinkgreve, R.B.J., Kappert, M.H., and Bonnier, P.G. (2007). "Hysteretic damping in a small-strain stiffness model." *Proceedings of the 10th International Symposium on Numerical Models in Geomechanics NUMOG 10—Numerical Models in Geomechanics NUMOG 10*, 737-742.

Brinkgreve, R., Engin, E., and Swolfs, W. (2013). *PLAXIS 3D 2019 Reference Manual*, Delfts, Netherland.

Do, T.N., Ou, C.Y., and Chen, R.P. (2016). "A study of failure mechanisms of deep excavations in soft clay using the finite element method." *Computers and Geotechnics*, **73**, 153-163. https://doi.org/10.1016/j.compgeo.2015.12.009

FUGRO (2018). *Geotechnical Report Pilot Geotechnical Site Investigation Seawall Earthquake Safety Program San Francisco,* FUGRO Corporation Report, California, 002(04).

Gibbs, J.F., Fumal, T.E., Borcherdt, R.D., Warrick, R.E., Liu, H., and Westerlund, R.E. (1994). *Seismic Velocities and Geologic Logs from Boreholes at Three Downhole Arrays in San Francisco, California*, U.S. Geological Survey Open-File Report, 94-706.

Hardin, B.O. and Black, W.L. (1969). "Vibration modulus of normally consolidated clay." *Journal of the Soil Mechanics and Foundations Division*, **94**(2), 353-369. https://doi.org/10.1061/jsfeaq.0001100

Hardin, B.O. and Drnevich, V.P. (1972). "Shear modulus and damping in soils: design equations and curves." *Journal of the Soil Mechanics and Foundations Division*, **98**(7), 667-692. https://doi.org/10.1061/JSFEAQ.0001760

Hsieh, P.G. and Ou, C.Y. (2018). "Mechanism of buttress walls in restraining the wall deflection caused by deep excavation." *Tunnelling and Underground Space Technology*, Elsevier, **82**(October 2017), 542-553. https://doi.org/10.1016/j.tust.2018.09.004

Jaky, J. (1944). "The coefficient of earth pressure at rest." *Journal of the Society of Hungarian Architects and Engineers*, **78**(22), 355-358

Khoiri, M. and Ou, C.Y. (2013). "Evaluation of deformation parameter for deep excavation in sand through case histories." *Computers and Geotechnics*, **47**, 57-67. https://doi.org/10.1016/j.compgeo.2012.06.009

Kulhawy, F.H. and Mayne, P.W. (1990). *Manual on Estimating Soil Properties for Foundation Design*, Cornell University, New York.

Kung, G.T., Juang, C.H., Hsiao, E.C., and Hashash, Y.M. (2007). "Simplified model for wall deflection and ground-surface settlement caused by braced excavation in clays." *Journal of Geotechnical and Geoenvironmental Engineering*, ASCE, **133**(6), 731-747. https://doi.org/10.1061/(ASCE)1090-0241(2007)133:6(731)

Lim, A. (2018). *Investigation of Integrated Buttress and Cross Walls to Control Movements Induced by Excavation*, Ph.D. Dissertation, National Taiwan University of Science and Technology.

Lim, A., Hsieh, P.G., and Ou, C.Y. (2016). "Evaluation of buttress wall shapes to limit movements induced by deep excavation." *Computers and Geotechnics*, **78**, 155-170. https://doi.org/10.1016/j.compgeo.2016.05.012

Lim, A. and Ou, C.Y. (2017). "Stress paths in deep excavations under undrained conditions and its influence on deformation analysis." *Tunnelling and Underground Space Technology*, **63**, 118-132. https://doi.org/10.1016/j.tust.2016.12.013

Lim, A., Ou, C.Y., and Hsieh, P.G. (2010). "Evaluation of clay constitutive models for analysis of deep excavation under undrained conditions." *Journal of GeoEngineering*, **5**(1), 9-20.

Lim, A., Ou, C.Y., and Hsieh, P.G. (2020). "A novel strut-free retaining wall system for deep excavation in soft clay: numerical study." *Acta Geotechnica*, Springer Berlin Heidelberg, **15**(6), 1557-1576. https://doi.org/10.1007/s11440-019-00851-5

Mana, A.I. (1980). *Finite Element Analyses of Deep Excavation Behavior in Soft Clay*. Ph.D. Dissertation, Stanford University.

Ou, C.Y. (2006). *Deep Excavation Theory and Practice*. Taylor & Francis. https://doi.org/10.1201/9781482288469

Ou, C.Y. (2015). "Finite element analysis of deep excavation problems." *Journal of GeoEngineering*, **11**(1), 1-12. http://dx.doi.org/10.6310/jog.2016.11(1).1

Ou, C.Y., Shiau, B.-Y., and Wang, I.-W. (2000). "Three-dimensional deformation behavior of the Taipei National Enterprise Center (TNEC) excavation case history." *Canadian Geotechnical Journal*, **37**(2), 438-448. https://doi.org/10.1139/t00-018

Ou, C.Y., Hsieh, P.G., and Lin, Y.L. (2013). "A parametric study of wall deflections in deep excavations with the installation of cross walls." *Computers and Geotechnics*, **50**, 55-65. https://doi.org/10.1016/j.compgeo.2012.12.009

Ou, C.Y., Lin, Y.L., and Hsieh, P.G. (2006). "Case record of an excavation with cross walls and buttress walls." *Journal of GeoEngineering*, **1**(2), 79-87.

Santos, J.A. and Correia, A.G. (2001). "Reference threshold shear strain of soil. Its application to obtain an unique strain-dependent shear modulus curve for soil." *Proceedings of the 15th International Conference on Soil Mechanics and Geotehcnical Engineering*. Istanbul, Turkey, **1**, 267-270.

Schanz, T., Vermeer, P.A., and Bonnier, P.G. (1999). "The hardening soil model: Formulation and verification." *Beyond 2000 in Computational Geotechnics. Ten Years of PLAXIS International. Proceedings of the International Symposium,* Amsterdam, March 1999, 281-296.

Shibuya, S. and Tanaka, H. (1999). "Estimate of elastic shear modulus in holocene soil deposits." *Soils and Foundations*, Elsevier Masson SAS, **39**(2), 45-55. https://doi.org/10.3208/sandf.36.4_45

Teng, F.C. (2010). *Prediction of Ground Movement Induced by Excavation Using the Numerical Method with Consideration of Inherent Stiffness Anisotropy*, Ph.D. Dissertation, National Taiwan University of Science and Technology.

Terzaghi, K. (1943). *Theoretical Soil Mechanics*, John Wiley & Sons, New York. https://doi.org/10.1002/9780470172766

Yeh, T., Ou, C.Y., and Lim, A. (2022). "A case study of strut-free excavation retaining system." *Acta Geotechnica*, Springer Berlin Heidelberg, 4. https://doi.org/10.1007/s11440-022-01526-4